Journal of
Ceramic Science
and Technology

J. Ceram. Sci. Tech., 02 [04] 211-216 (2011)
DOI: 10.4416/JCST2011-00035
available online at: http://www.ceramic-science.com

Injection Molding of Alumina-Chromia-Yttria Composites

F. Sommer*, F. Kern, R. Gadow

University of Stuttgart, Institute for Manufacturing Technologies of Ceramic Components and Composites, D-70569 Stuttgart, Allmandring 7b, Germany

received September 21, 2011; received in revised form October 19, 2011; accepted October 26, 2011

Abstract

A submicron alumina powder was co-doped with chromia and yttria in order to obtain a homogeneous microstructure with grain boundaries strengthened by yttrium aluminium garnet (YAG) precipitates and a solid solution of chromia in alumina leading to high hardness and enhanced fracture toughness. The ceramic injection molding (CIM) process was applied as one of the most high-performance technologies for complex components and near-net-shape series production capability. To ensure the production of samples without defects, the injection parameters were optimized. CIM specimens were pressurelessly sintered in a hydrogen atmosphere in order to avoid chromium trioxide evaporation and improve sinterability. Materials with a bending strength of 570 MPa and a fracture toughness of 3.52 MPa√m (Evans) were obtained.

Keywords: Alumina, yttria, YAG, composite, injection molding

I. Introduction

Alumina-based composites produced by adding second phases, either immiscible (zirconia, silicon carbide) or miscible phases (yttria, magnesia, titania), have led to materials with improved properties [1]. YAG formed from yttria is known to hinder grain growth during sintering, which allows the production of materials with microstructures in the sub-micron range [2,3]. The alumina-YAG system has recently attracted considerable interest, as materials with increased strength, toughness and creep resistance can be obtained [4,5,6]. The increase in toughness can be partially attributed to a YAG layer around the alumina grains, which strengthens grain boundaries and changes crack propagation from the intergranular to transgranular mode [7]. The manufacturing and mechanical properties of Al_2O_3/5 – 30 vol% YAG were systematically studied [8]. One problem associated with the production of alumina-YAG from the oxides by means of reaction sintering is the intermediate formation of monoclinic (YAM) or perovskite type (YAP) yttrium aluminates, which cause problems during sintering. Uncertainties concerning these intermediate phases existed until Cockayne successfully proved the stability of these phases at room temperature [9,10]. In the case of yttria-coated alumina powders, the problem can be solved by subjecting the starting powder to complex heat treatment cycles, which are difficult to scale up [11]. Yttrium chromite as an yttria and chromia precursor for the simultaneous hardening and stabilization of ZTA avoiding un-derived intermediate phases by controlled release of Y_2O_3 and Cr_2O_3 from a ternary phase has been demonstrated by Burger [12]. The feasibility to produce alumina-yttria-chromia nanocomposites (ACY) from different alumina powders and $YCrO_3$ by hot pressing was recently shown by the authors [13]. Two different alumina powders were doped with 5 wt% yttrium chromite and subsequently hot-pressed at temperatures between 1400 °C and 1600 °C at 60 MPa and one hour dwell in vacuum. All relative densities were above 98 % of the theoretical densities. Maximum HV_{10} values of 1935 ± 22 and bending strength of 542 ± 30 MPa were achieved. Indentation fracture toughness of 4.85 ± 0.15 MPa√m (Niihara) up to 5.73 ± 0.34 MPa√m (Niihara) varied depending on sintering temperatures. For better comparison, these fracture toughness values correspond to 2.95 MPa√m and 3.87 MPa√m (Evans), respectively. The aim of this new study is to transfer the hot pressing findings to ceramic injection molding (CIM), a high-performance manufacturing technology capable of forming complex-shaped engineering ceramics.

II. Experimental

Yttrium chromite $YCrO_3$ was produced by means of reaction-sintering nanoscale yttria (99.99 %, Sigma Aldrich) and chromia powders (produced from chromium acetate hydroxide) at 1200 °C/2 h in a hydrogen atmosphere. $YCrO_3$ was blended with an α-alumina (Sasol, North America, S_{BET} 8 m²/g, d_{50} = 0.3 μm) in a ratio of 2.5/97.5 wt%. The manufacturer's data were verified by means of laser granulometry (Malvern Lasersizer), SEM images were taken of $YCrO_3$ and alumina.

The feedstock was prepared according to a procedure previously described in detail [14]. Three kilograms of thermoplastic feedstock consisting of 85 wt% of the powder blend and 15 wt% of commercially available binder was produced. The molding process was performed on a hy-

* Corresponding author: frank.sommer@ifkb.uni-stuttgart.de

draulic injection molding machine (Boy50M, Dr. Boy, Germany). Test plates with a size of 35 × 45 × 3 mm³ were produced. The applied molding parameters were an injection pressure of 1000 bar and injection speed of 10 – 30 cm³/s, a packing pressure of 500 bar, a plastification temperature of 140 – 155 °C, a mold temperature of 65 °C and a cooling time of 20 s.

The samples were then debinded in two-step debinding process. The water-soluble fraction was removed by extraction in water at 60 °C for 12 h. The residual binder was burnt out in air. DTA/TG measurements (Netzsch, STA 409 CD) were conducted to set up the debinding parameters. Before final sintering, all samples were pre-sintered at 800 °C for 24 h in air.

The porosity distribution of the pre-sintered green bodies was monitored by means of mercury intrusion porosimetry (Pascal 140/440, Porotec GmbH, Germany), the microstructure of fractured green bodies was investigated with SEM (Leo VP 438) in order to detect inhomogeneities in the microstructure.

All samples were subsequently sintered in a hydrogen atmosphere (Xerion, Freiberg, Germany). Sintering temperatures varied between 1425 °C and 1475 °C, with a heating rate of 2 K/min and dwell times from 60 min up to 180 min. After sintering, the samples were fine-ground with a 40-μm diamond disk before polishing with 15-μm, 6-μm, 3-μm and 1-μm diamond suspension.

The density of all specimens was determined with the Archimedes method. For 3-point bending tests, five test bars each of the polished samples were cut and the edges of the samples were carefully beveled. Then bending tests were performed according to DIN EN 6872. Microhardness ($HV_{0.1}$) was tested with a Fischerscope microindenter on a polished surface (Fischer, Sindelfingen, Germany). The indentation modulus was calculated from the indentation curve according to the universal hardness method. Hardness (HV_{10}) was measured with the Vickers indentation method, whereupon fracture toughness was calculated with Evans' formula [15] from the length of the cracks of the HV_{10} measurements. It should be noted that absolute toughness values measured by indentation are not as reliable as toughness values examined, for example, with the SEVNB or ISB method [16], but the values are sufficient to compare results within a study. The microstructures and fracture faces of the sintered specimen were investigated with SEM. The phase composition of polished surfaces was determined with X-ray diffraction (XRD) (Bruker D8, Germany) using CuKα radiation with a graphite monochromator in order to confirm the YAG phase formation.

III. Results and Discussion

Laser granulometry measurements confirmed the manufacturer's data for the alumina exactly. SEM images of the starting alumina and $YCrO_3$ powder are shown in Figs. 1 and 2. SEM images of Al_2O_3 revealed particles with spherical morphology suitable for injection molding. The $YCrO_3$ powder has particle sizes of around 1 μm with some 4-μm agglomerates.

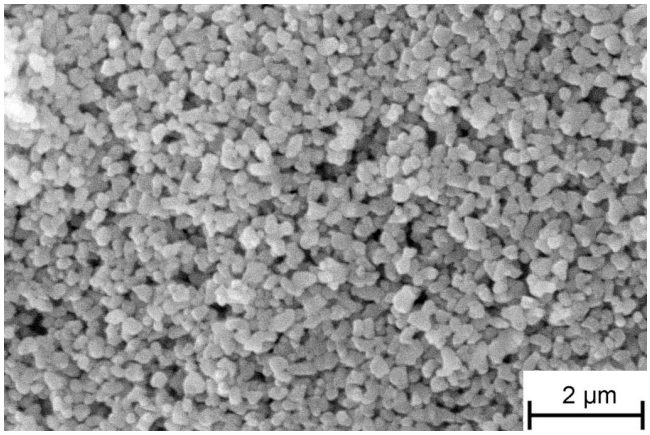

Fig. 1: SEM image of starting alumina powder.

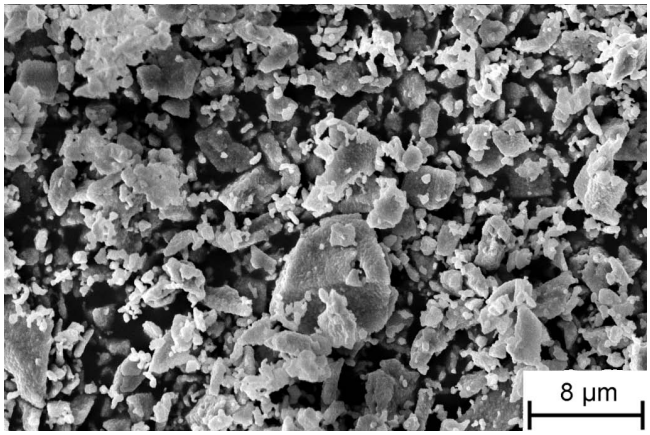

Fig. 2: SEM image of reaction-sintered yttrium chromite powder.

Some basic injection parameters were kept constant during the optimization of the molding process. Eightcubic centimeters of injection volume was necessary to fill the mold cavity. The screw rotational speed was set at 150 min^{-1}, the clamping force of the mold was 300 kN. Other injection parameters had to be optimized in order to produce perfect plates without visible defects like voids or cracks.

The best molding results were obtained at an injection speed of 25 cm³/s (pressure of 1000 bar) and a packing pressure of 500 bar. With lower injection pressure, the edge region of the plates was not duly completed. To avoid an uneven surface, a packing pressure of minimum 500 bar had to be applied. Another critical parameter was the injection speed. At a slower injection speed than 10 cm³/s, the cavity was not filled completely and short shots occurred, injection speed > 30 cm³/s caused various surface defects, e.g. jetting, cracks or voids. The plastification temperature was set to 140 – 155 °C, with increasing temperature towards the nozzle. To support the filling of the cavity, the mold temperature was raised up to 65 °C. Cooling time was 20 s. Higher mold temperatures caused undesired sticking effects.

A two-step debinding process was applied. Solvent debinding in water at 60 °C/24 hours generates an open pore network for the subsequent binder burn-out. Thermal debinding with subsequent pre-sintering at 800 °C/24 h was conducted to remove the residual binder and provide a homogeneous microstructure und sufficient component stability. Pre-sintered samples could be transferred

to the final sinter furnace without any damage. DTA/TG measurements were used to set up an appropriate debinding process for ACY ceramics. A static air atmosphere and a heating rate of 5 K/min were applied to simulate realistic debinding parameters without running the risk of base-line drifting at heating rates that are too low. If we look at DTA/TG graphs, it is obvious that measurements of the pure binder will not lead to successful debinding parameters because debinding characteristics change once the binder is dispersed in the ceramic green body. However, complete binder volatilization without residuals is noticeable as the TG binder graph reaches the zero level. In the ACY green body, binder degradation starts at 220 °C and is finished at around 440 °C (Fig. 3). The derivative of the thermal gravimetric analysis showed a maximum decomposition rate at temperatures around 255 °C. Nevertheless, the huge difference in dimension between the DTA/TG specimen and the real injection-molded samples should be taken into consideration. For smooth debinding, dwell steps should be inserted to enable homogenous heat transfer within the sample and slow volatilization of the binder. This is why the heating rate was reduced to 10 K/h, hence the maximum temperature can be reduced to 380 °C. According to DTA/TG measurements, thermal debinding parameters were set to 12-h dwell at 380 °C with an applied heating rate of 10 K/h and subsequent pre-sintering at 800 °C for 24 h at heating rate of 60 K/h. The thermogravimetry graph of the ACY sample shows a mass loss of 10.5 wt%. Thus with the original addition of 15 wt% binder to the composition, 4.5 wt% were removed during water debinding. This is the equivalent to 30 vol% of the binder, which agrees with the proposition of German [17] for the creation of an open pore network while avoiding cracking and blistering during thermal debinding.

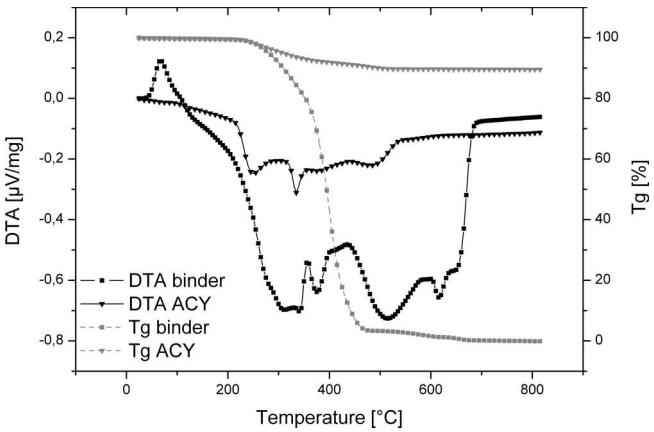

Fig. 3: DTA and TG of pure binder and water-debinded ACY.

The pore size distribution and SEM image of the debinded and pre-sintered ACY samples are shown in Figs. 4 and 5. Pore radii were between 0.023 and 0.076 micrometer as expected. A single narrow peak indicates a defect-free microstructure. SEM images of fracture faces of thermally debinded samples show some small internal voids, which were not detected by mercury intrusion. Dilatometry (not shown) was performed in argon and air. In neither of these atmospheres was it possible to completely densify the samples. The onset of sintering was at 1100 °C, maximum densification rate was reached at 1450 °C. The sintering temperatures were thus set between 1425 °C to 1475 °C, dwell was 60 – 180 min. The temperature range for optimum densification is in good accordance with results published by Palmero [18]. A hydrogen atmosphere was chosen to facilitate densification and prevent evaporation of CrO_3.

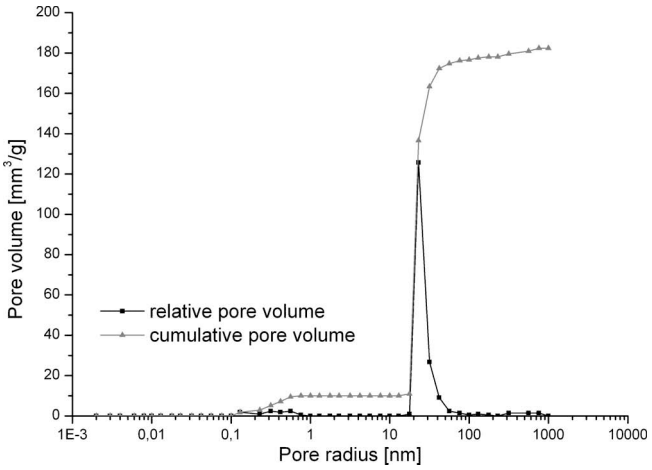

Fig. 4: Pore size distribution of ACY in thermally debinded state determined by means of mercury intrusion.

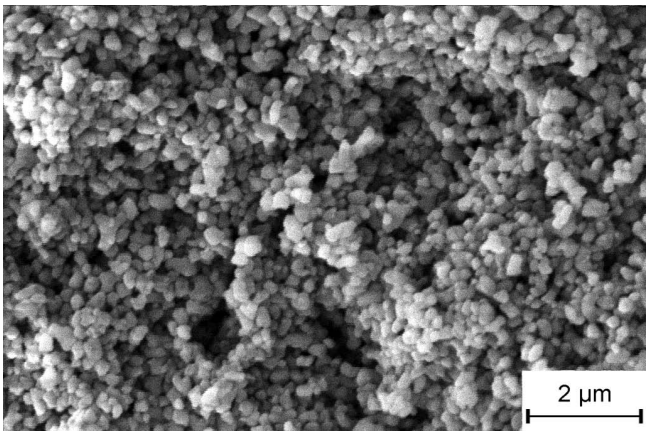

Fig. 5: SEM image of the microstructure of a fracture face of thermally debinded ACY.

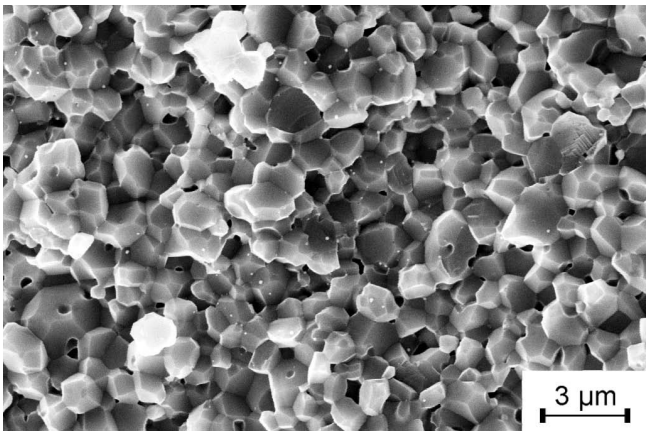

Fig. 6: Fracture surface of ACY specimen, sintered at 1425 °C, 90 min dwell.

Figs. 5 – 10 show SEM images of the fracture faces of ACY specimens, sintered at different temperatures and

dwell times. SEM images of the microstructure showed incompletely densified samples with small grain sizes of about one to two microns. Up to 1450 °C, yttria was effective in hindering grain growth while at higher temperatures or very long dwell times the alumina grains grew considerably to 3 – 10 μm. From fracture surfaces the different fracture mechanisms can be clearly seen. When bigger grains are noticeable, besides intergranular cracking also transgranular cracking appears. This should result in an enhancement of toughness, when the microstructure is carefully adjusted and both cracking mechanisms occur.

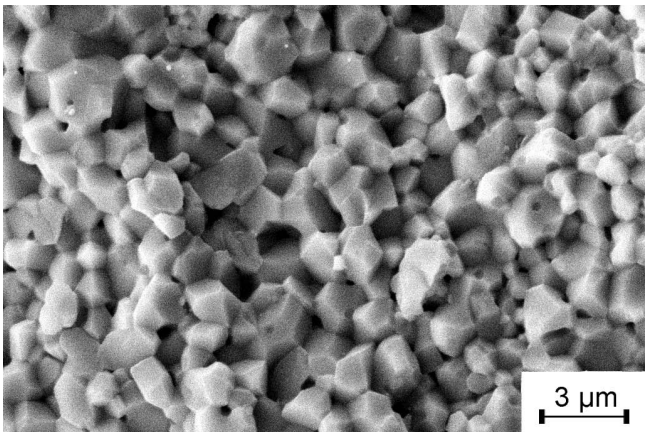

Fig. 7: Fracture surface of ACY specimen, sintered at 1450 °C, 90 min dwell.

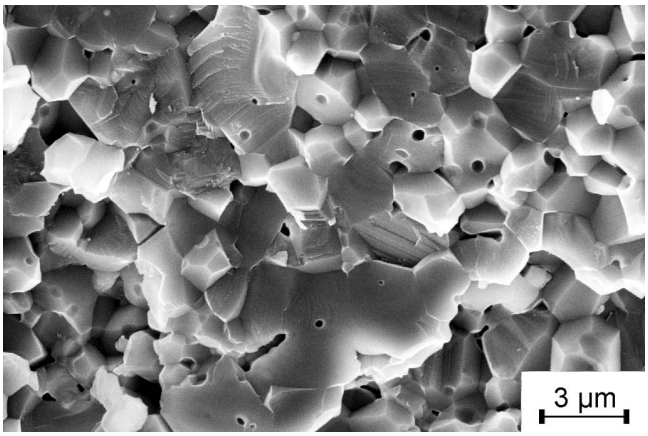

Fig. 8: Fracture surface of ACY specimen, sintered at 1475 °C, 90 min dwell.

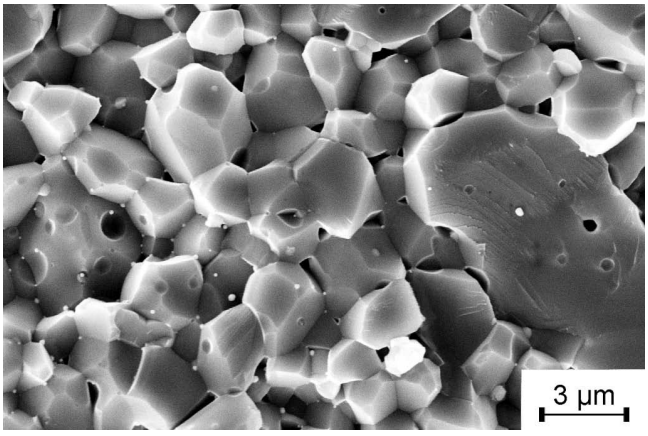

Fig. 9: Fracture surface of ACY specimen, sintered at 1450 °C, 180 min dwell.

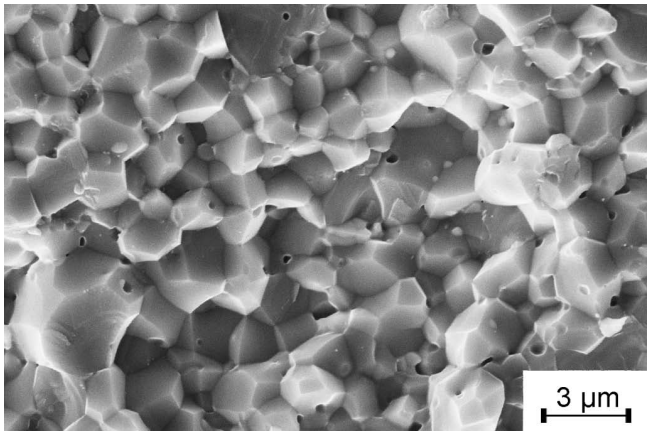

Fig. 10: Fracture surface of ACY specimen, sintered at 1475 °C, 60 min dwell.

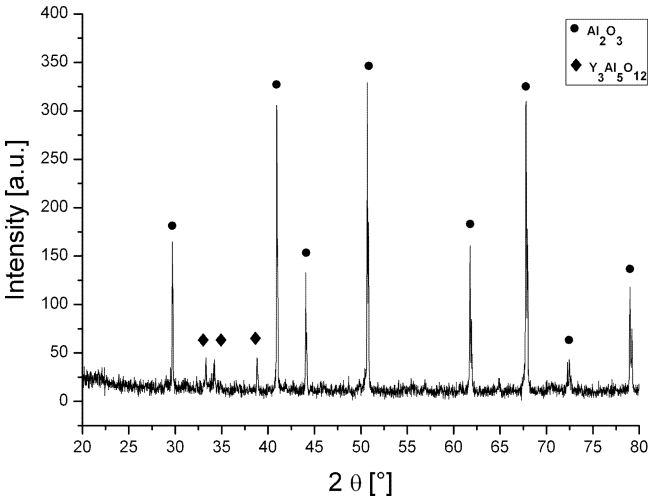

Fig. 11: XRD pattern of polished ACY specimen, sintered at 1450 °C, 180 min dwell.

Fig. 11 shows an XRD pattern of a polished ACY specimen, sintered at 1450 °C with 180-min dwell. Only two phases were observed, α-alumina and the YAG phase. Neither monoclinic (YAM) nor perovskite type (YAP) yttrium aluminate phase was detectable. This confirms the successful approach of $YCrO_3$ doping for the formation of alumina-YAG composites.

Table 1 shows all measured mechanical properties of the ACY injection-molded specimen. Relative densities were about 96 %, which confirms results already seen in SEM images. Evidently the processing range for sintering is very narrow. If the sintering temperature is too low at 1425 °C, incomplete densification and low hardness result. Increasing the sintering temperature to 1450 °C at identical dwell leads to higher density and high hardness while strength and toughness are hardly affected. The best results were obtained at 1475 °C and 90 min dwell. While densification does not progress further, strength and toughness rise to the highest levels of 568 MPa and 3.52 MPa√m. Owing to the larger grain sizes a slight decline in hardness is observed.

Table 1: Mechanical properties of the ACY injection-molded specimen.

Samples	rel. density	$HV_{0.1}$	Ind. modulus	HV_{10}	K_{1C} (Evans)	Bending strength
	[%]	[kp/mm^2]	[GPa]	[kp/mm^2]	[MPa√m]	[MPa]
1425 °C, 90 min	94.40±0.24	1814±139	350±13	1807±118	3.29±0.46	488±29
1450 °C, 90 min	96.75±0.09	2203±62	409±5	1987±63	2.82±0.15	495±87
1475 °C, 90 min	96.64±0.17	2160±81	392±10	1852±82	3.52±0.18	568±50
1450 °C, 180 min	96.24±0.17	2080±157	361±17	1714±54	3.35±0.20	479±107
1475 °C, 60 min	96.01±0.41	2218±89	395±7	1909±91	3.36±0.24	435±194

IV. Conclusion

Co-doping of alumina with yttria and chromia derived from an $YCrO_3$ precursor is a feasible method to form YAG precipitates. In comparison with hot pressing, where pressure supports densification, it is difficult to completely densify injection-molded ACY samples. Longer dwell times and hydrogen sintering effects densification but relative densities still remained below 97 %. Further densification could be achieved with subsequent post-hipping. In order to produce components with high dimensional accuracy, injection parameters have to be carefully adjusted. When appropriate debinding parameters are selected, injection-molded samples are not destroyed within this critical process step. Sintering has to be performed in hydrogen within a very narrow final temperature/dwell level range to obtain materials with optimum strength and toughness. In comparison with hot-pressed ACY materials, the mechanical properties show similar maximum values for fracture toughness and bending strength with little loss in hardness. Other alumina-YAG composites manufactured by means of conventional uniaxial and isostatic pressing and similar composition do not outreach properties achieved in this study. Lach reported a hardness of 1943 ± 0.57 GPa, a bending strength of 232 ± 18 MPa and an indentation fracture toughness of 4.39 ± 0.52 MPa√m (Niihara) for a similar material composition [8]. The results of the previous study were successfully implemented in ceramic injection molding (CIM), which offers higher design flexibility, but no significant loss in mechanical properties.

References

1 Sternitzke, M.: Review: structural ceramic nanocomposites, *J. Eur. Ceram. Soc.*, **17**, 1061 – 1082, (1997).

2 Cinibulk, M.K.: Effect of yttria and yttrium-aluminum garnet on densification and grain growth of alumina at 1200°–1300 °C, *J. Am. Ceram. Soc.*, **87**, 692 – 695, (2004).

3 Voytovych, R., MacLaren, I., Gülgün, M.A., Cannon, R.M., Rühle, M.: The effect of yttrium on densification and grain growth in α-alumina, *Acta Mater.*, **50**, 3453 – 3463, (2002).

4 Palmero P., Naglieri, V., Chevalier, J., Fantozzi, G., Montanaro, L.: Alumina-based nanocomposites obtained by doping with inorganic salt Solutions: application to immiscible and reactive systems, *J. Eur. Ceram. Soc.*, **29**, 59 – 66, (2009).

5 Parthasarathy, T.A., Mah, T., Matson, L.E.: Processing, structure and properties of Alumina-YAG eutectic composites, *J. Ceram. Process. Res.*, **5**, 380 – 390, (2004).

6 Mah, T., Parthasarathy, Lee, H.D.: Polycrystalline YAG: structural or functional, *J. Ceram. Process. Res.*, **5**, 369 – 379, (2004).

7 Cannillo, V., Palmero, P., Manfredini, T., Montanaro, L.: Alumina-YAG composites: Preparation, experimental characterisation and numerical modelling, *Int. J. Mater. Prod. Tech.*, **35**, (2009).

8 Lach, R., Haberko, K., Bucko, M.M., Szumera, G., Grabowski, G.: Ceramic matrix composites in the Alumina/5 – 30 vol% YAG system, *J. Eur. Ceram. Soc.*, **31**, 1889 – 1895, (2011).

9 Cockayne, B.: The Uses and Enigmas of the Al_2O_3-Y_2O_3 Phase System, *J. Less Common Met.*, **114**, 199 – 206, (1985).

10 Mah, T., Petry, M.: Eutectic composition in the pseudobinary of $Y_4Al_2O_9$ and Y_2O_3, *J. Am. Ceram. Soc.*, **75**, 2006 – 2009, (1992).

11 Naglieri, V., Joly-Pottuz, L., Chevalier, J., Lombardi, M., Montanaro, L.: Follow-up of zirconia crystallization on a surface modified alumina powder, *J. Eur. Ceram. Soc.*, **30**, 3377 – 3387, (2010).

12 Burger, W., Richter, H.G.: High strength and toughness alumina matrix composites by transformation toughening and '*In Situ*' platelet reinforcement (ZPTA) – The new generation of bioceramics, *Key Eng. Mat.*, **192 – 195**, 545 – 548, (2001).

13 Sommer, F., Kern, F., Gadow, R., Hot-pressing of Yttria-Chromia Al_2O_3 Composites, Proc. CIEC, **12**, S2.

14 Kern, F., Gadow, R.: Extrusion and injection molding of ceramic micro and nano composites, *Int. J. Mater. Form.*, **2**, 609 – 612, (2009).

15 Evans, A.G., McMeeking, R.M.: Mechanics of transformation-toughening in brittle materials, *J. Am. Ceram. Soc.*, **65**, 242 – 246, (1982).

16 Quinn, G.D., Bradt, R.C.: On the vickers indentation fracture test, *J. Am.Ceram. Soc.*, **90**, 673 – 680, (2007).

17 German, R.M.: Powder injection molding, Metal Powder Industries Federation, Princeton, New Jersey, (1990).

18 Palmero, P., Kern, F., Lombardi, M., Gadow, R.: Role of immiscible and miscible second phases on the sintering kinetics and microstructural development of nano-crystalline α-Al_2O_3-based materials, *Ceram. Int.,* (2011), doi: 10.1016.jceramint.2011.06.011